Micro- and macro-structural heterogeneities in 316L stainless steel prepared by electron-beam melting

Olsén, Jon; Shen, Zhijian; Liu, Leifeng; Koptyug, Andrey; Rännar, Lars-Erik

DOI:
10.1016/j.matchar.2018.04.026

Document Version
Peer reviewed version

Citation for published version (Harvard):
Olsén, J, Shen, Z, Liu, L, Koptyug, A & Rännar, L-E 2018, 'Micro- and macro-structural heterogeneities in 316L stainless steel prepared by electron-beam melting', *Materials Characterization*, vol. 141, pp. 1-7. https://doi.org/10.1016/j.matchar.2018.04.026

Accepted Manuscript

Micro- and macro-structural heterogeneities in 316L stainless steel prepared by electron-beam melting

Jon Olsén, Zhijian Shen, Leifeng Liu, Andrey Koptyug, Lars-Erik Rännar

PII:	S1044-5803(18)30395-4
DOI:	doi:10.1016/j.matchar.2018.04.026
Reference:	MTL 9166
To appear in:	*Materials Characterization*
Received date:	19 February 2018
Revised date:	16 April 2018
Accepted date:	17 April 2018

Please cite this article as: Jon Olsén, Zhijian Shen, Leifeng Liu, Andrey Koptyug, Lars-Erik Rännar , Micro- and macro-structural heterogeneities in 316L stainless steel prepared by electron-beam melting. The address for the corresponding author was captured as affiliation for all authors. Please check if appropriate. Mtl(2017), doi:10.1016/j.matchar.2018.04.026

Micro- and macro-structural heterogeneities in 316L stainless steel prepared by electron-beam melting

Jon Olsén [a*], Zhijian Shen [a], Leifeng Liu [b], Andrey Koptyug [c], Lars-Erik Rännar [c]

[a] Stockholm University, Arrhenius Laboratory, Svante Arrhenius väg 16 C, SE-10691, Stockholm, Sweden

[b] University of Birmingham, Metallurgy and Materials, Pritchatts Road, Birmingham B15 2TT, United Kingdoms

[c] Mid Sweden University, Sports Tech Research Centre, Akademigatan 1, SE-83125, Östersund, Sweden

[*] Corresponding author. jon.olsen@mmk.su.se

Abstract

This is a study of the micro- and macrostructural variations in samples of stainless steel with the overall composition of the grade 316L, produced using electron beam melting. Electron beam melting is one of the processing methods under consideration for manufacturing some of the International Thermo- Nuclear Experimental Reactor In-Vessel components. Therefore further studies of the homogeneity of the material were conducted. Electron beam melting results in a complicated thermal history of the manufactured part giving a significant impact on the microstructure. A cellular structure that is often observed in samples prepared by selective laser melting was found in the top layers of the specimens. Further down, the structure changed until the cellular structure was almost non-existing, and the grain boundaries had become more pronounced. This revelation of a heterogeneous structure throughout the entire part is crucial for large-scale industrial applications like the Thermo-Nuclear Experimental Reactor to make sure that it is understood that the properties of the material might not be the same at every point, as well as to assure that the correct post-treatment is done. It is also exposed that a significant part of this change is due to molybdenum redistribution inside the sample when it diffuses from the cell boundaries into the cells, and into bigger agglomerates in the grain boundaries. This diffusion seems not to affect the microhardness of the samples.

Keywords: Additive manufacturing, Electron beam melting, Microstructure, 316L stainless steel, Heterogeneous material

1. Introduction

Additive manufacturing (AM), also known as 3D-printing, has historically mostly been used for fast prototyping of parts and tools[1]. When using AM, it is possible to move from idea to an industrial prototype quickly. In recent time this has changed, and many actors have started to use AM also as an industrial production tool, and not only a prototyping tool[2,3]. As AM becomes more commonly used for real applications, understanding of the process and the microstructure of the resulting material becomes crucial. Stainless steel structures manufactured with selective laser melting (SLM) have already been characterized and

manipulated to a high degree, but for electron beam melting (EBM®), very few sources describing the resulting structures can be found[4–6]. Though both methods belong to the powder-bed AM technology family, there are specific differences in both machine layout, process settings and, as a result, in the microstructure of the produced components. The EBM® process is a bottom-up process using a high power electron beam to melt powder adding one layer of material at a time. During the preparation stage, a CAD file depicting the desired geometry is produced. Next, specialized software is used to slice the images into several layers. During manufacturing, a high energy electron beam is scanned over the surface of the powder layer, melting the powder. As more layers are added, the previous layers are re-melted or partially re-melted several times, resulting in a complex cycle of melting and solidification, this, in turn, enables the formation of a complex heterogeneous microstructure.

Stainless steel with the overall composition of the grade 316L prepared by electron beam melting is one of the materials considered for use in the International Thermo- Nuclear Experimental Reactor (ITER project) and in other critical industrial applications. Therefore a more in-depth knowledge of the microstructure and its dependence on the processing parameters are desirable. Samples manufactured with EBM® have a thermal history unlike both traditionally manufactured bulk parts and parts manufactured using laser-based AM technologies[7–9]. The main difference is not only the layer-by-layer melting-annealing of the material but also the prolonged exposure of components to elevated temperatures during EBM®-manufacturing. During the EBM® process, the components and surrounding powder are held at a temperature around 800°C. Moreover, the first layers of material are kept at these temperatures much longer than the last ones in the build, and this could influence the microstructure of the components differently at different locations, resulting in a structural gradient that permeates the entire component. The input energy from the electron beam is also higher than that from the laser beam which results in a higher amount of energy that needs to be conducted away from the beam impact area. In this study, materials taken from different locations of the EBM®-manufactured components are examined to determine the microstructural effects of the unique thermal history of the samples produced.

2. Material and process

2.1 Precursor material

The precursor material was a gas atomized spherical 316L powder from Carpenter Powder products AB (Torshälla, Sweden) with a composition shown in Table 1. The powder was mostly spherical with only a small number of 'satellites,' and a grain size distribution between 53 and 150μm. Just a few more substantial grains, mainly representing a few sub-grains bonded together are present (Figure 1). Powder bed fusion systems such as EBM® have certain demands to the powder flowability and apparent density to guarantee low porosity and uniform quality of the manufactured material. Used powder has the flowability of 15.5 s/50g according to the ASTM B213, and the apparent density of 4.32 g/cm^3, which is within the range suggested by the EBM® machine manufacturer.

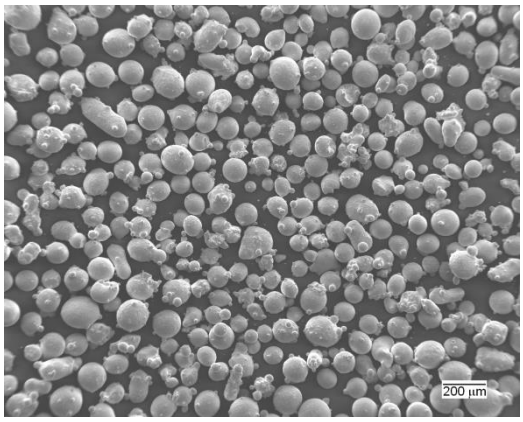

Figure 1. SEM image of the precursor powder.

Table 1. Chemical composition from the powder manufacturer

Element	C	Si	Mn	P	S	Fe	Cr	Ni	Mo	Cu	N	B	O
wt.%	.015	.45	1.75	.009	.005	65.4	17.6	12.2	2.51	.01	.080	.001	95ppm

2.2 Electron beam melting process

Manufacturing of the samples was done using ARCAM A2 machine (ARCAM AB, Mölndal, Sweden) operating at high vacuum. During the process temperature of the working area is kept constant by the internal feedback system to provide stable melting conditions. Samples were manufactured with a target process temperature of 800°C for the building plate during the entire build duration. Processing parameters were optimized for 70µm layer thickness and to give an entirely dense material, each layer taking between 70 to 90 seconds each to conclude, including the stages; pre-heating, melting of bulk material, melting of contours and post-heating. The whole build plate was of a dimension of 150*150mm with several different parts being spread across it, manufactured simultaneously. Overall build height for all components was 55mm with no supporting structure being used, and the parts being built directly on the building plate. The total built time was 20.4 hours before the helium is introduced into the chamber, allowing the system to cool down to room temperature for another 6 hours. In this study, two samples were used from this build: one with the dimensions 5*5*55mm and another with the dimensions 15*15*55mm, only the inner bulk part which was manufactured using single beam was investigated.

2.3 Characterization methods

Etching using Kroll's reagent (a mixture of 92 vol.% water, 6 vol.% concentrated Nitric acid, and 2 vol.% concentrated Hydrofluoric acid) was performed to enhance the visibility of melt-pool, grain, and cell boundaries. XRD analysis was carried out suing a PANalyticalX'Pert alpha1 diffractometer using a Kopper Kα radiation source. Before XRD measurements were carried out, the samples were thoroughly polished but not etched. The SEM images were taken in a JEOL JSM-7000F field emission scanning electron microscopy (SEM, JEOL, Tokyo, Japan). The EDS analysis was conducted using a TM3000 Tabletop SEM (Hitachi High-Technologies, Tokyo, Japan).

3. Results and discussion

3.1 Phase and predominant crystal growth directions

From the XRD pattern, initial insight into the phase composition and the crystal growth orientations can be gained. The precursor powder has a pure Austenite phase composition, and this is also expected in the EBM® manufactured sample. Looking at the XRD patterns (Figure 2) of the electron beam melted 316L stainless steel, reveals what appears to be a pure austenitic phase in the entire sample. This observation is consistent with earlier studies[4]. When performing XRD investigations at different heights in the sample, no noticeable difference is detected. The preferred crystal growth direction throughout the sample is along the (200) direction, which is coinciding with the build direction (Z-axis of the sample). The preferred growth direction in a fast cooling system is generally in the direction of the highest temperature gradient; this has been discussed in earlier studies[10]. Electron backscatter diffraction (EBSD) investigation of the samples shows the same results as XRD (Figure 3). The preferred crystal growth direction is in the (100) direction, with close to pure austenite phase. Comparing the texture of the EBM sample with a welded sample, where the preferred crystal growth direction is (111)[11], this reinforces the impression that EBM can produce components with a unique material microstructure and thus unique properties. A detailed analysis of the EBSD results gives a clear indication that the sample consists of more than 99.5% austenite phase, with a small fraction of ferrite and cementite mixture.

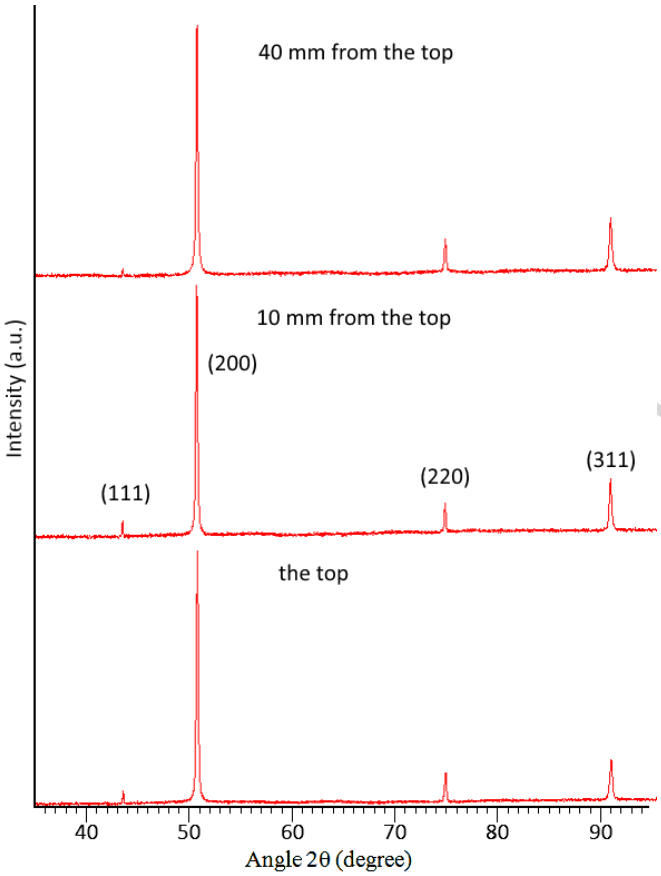

Figure 2. XRD pattern taken at three different building heights in the sample.

3.2 Grain size and grain morphology

Based on EBSD images, analysis of the grain size distribution was conducted. No definite difference could be detected among different areas along the sample height. The mean sizes of the grains were about 8μm across (normal to the build direction), but actual grain size variation is rather significant. Figure 3 presents typical grain morphology observed along (A), and normal to (B) the build direction, respectively. The grains are elongated along the build direction with lengths of up to 1 mm, indicating that the grains can grow through several layers by an epitaxial growth mechanism. This phenomenon is also present in parts built from other alloys[12,13], as well as 316L samples prepared by selective laser melting [14,15].

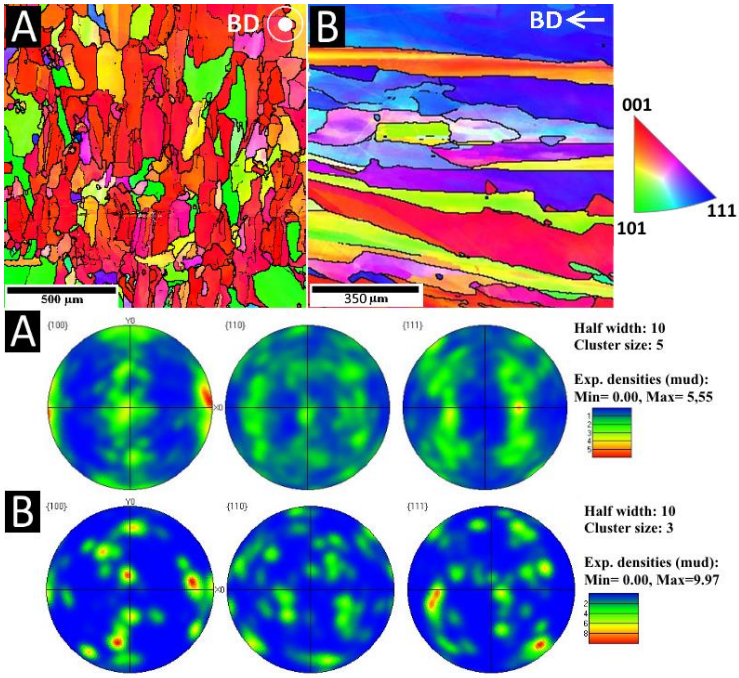

Figure 3. EBSD images of the EBM specimen with respective pole figure: (a) a top-down view, (b) a side view.

3.3 Optical microscope imaging

Optical microscopy investigation was carried out using the polished and etched samples. It revealed clear differences in the microstructure depending on the distance from the top surface (Figure 4). At the top, a commonly observed structure for some AM manufactured materials can be seen with evident traces of melt pools formed during the layer by layer manufacturing procedure. At higher magnification, the cellular structure can also be discerned (Figure 5A) as a shifting gray color on the surface. Moving down from the top layers, the structure gradually changes; the melt pool boundaries become blurrier, and the cellular structure fades away and finally disappears, revealed as a white color covering the sample (Figure 5B). The grain boundaries are also appearing more distinct at the bottom of the build. Cells and melt pools are the elements of structural heterogeneity introduced during the AM process because of the rapid thermal dynamics of the process (fast heating and cooling of the melt and surrounding areas). Local equilibrium is not attained during the narrow time window that the metal is in the liquid phase since this time is not adequate to allow for efficient diffusion. The observation that less of these elements appear closer to the build plate indicates that the structure there is less heterogeneous and much closer to a state of local chemical equilibrium.

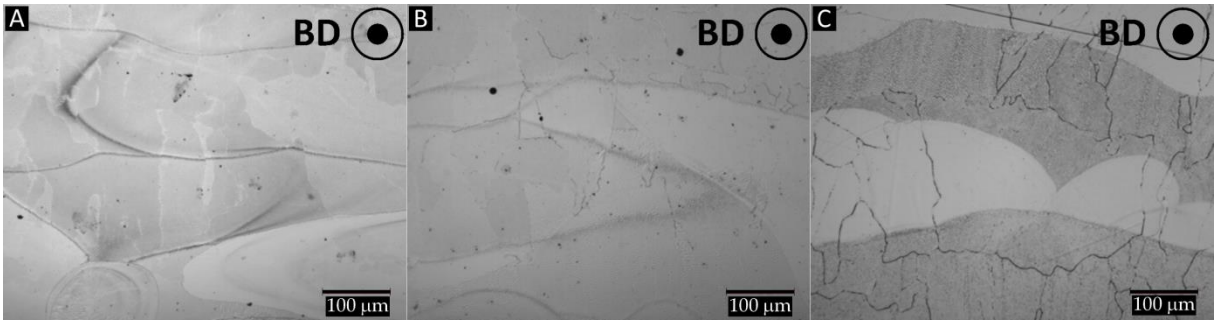

Figure 4. Top-down view of; (A) Top surface (B) 10mm from the top (C) 40mm from the top, showing a gradual change in the microstructural features.

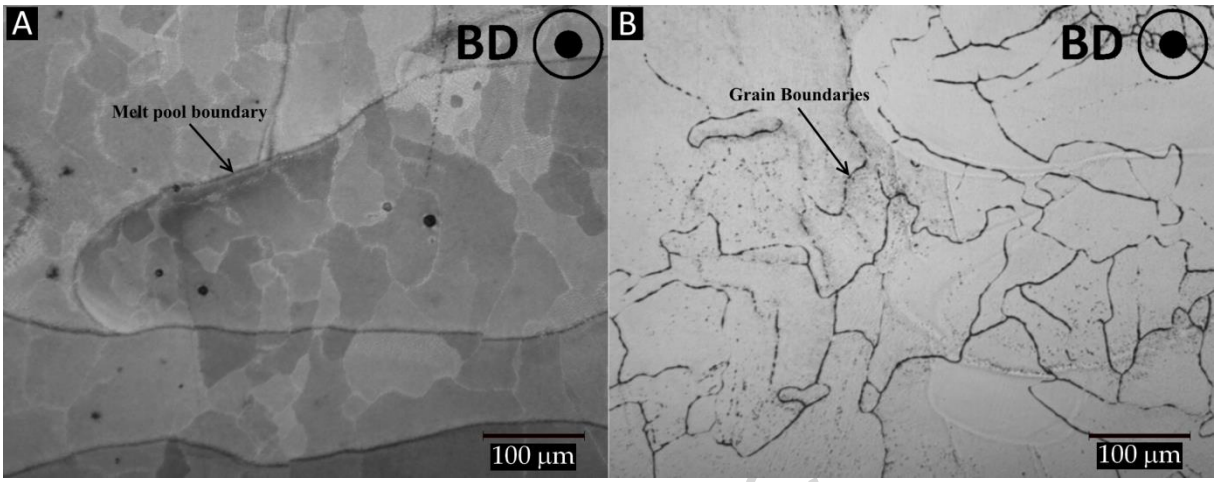

Figure 5. Top-down view at; (A) Top surface (B) 50mm from the top, at higher magnification showing the comparison in microstructure between the top and the bottom of the sample.

3.4 Segregation of Molybdenum

From the SEM images of the etched sample, the microstructure can also be seen changing with the distance from the top (Figure 6). At the top surface, the typical cellular structure is observed. This structure has earlier been reported for both SLM and EBM®[4,7,8]. The next image was taken 5 mm from the top surface and also shows a cellular structure, but the cell boundaries are thicker than at the top and not as pronounced. Further down, as can be seen in Figure 6F, the cells are hardly distinguishable. Figure 6G-L show the change in cellular structure observed in the direction perpendicular to the build direction. The same phenomenon as can be seen in viewing the sample along the build direction, the gradual disappearance of the cellular boundaries, is detected in the side view as well. An additional observation in this view is the agglomeration of white precipitates in the grain boundaries further from the surface. The brighter contrast, when using Backscatter detector in SEM investigations indicates heavier elements, in this case in the cell boundaries and the precipitates (Figure 7).To verify what the precipitates consist of, an EDS analysis was carried out. Table 2 shows the results of the EDS measurements, indicating that Molybdenum content in the investigated area increased by approximately 100% compared to the precursor powder. This gives a clear indication that Molybdenum segregation is a major part of the change in microstructure.

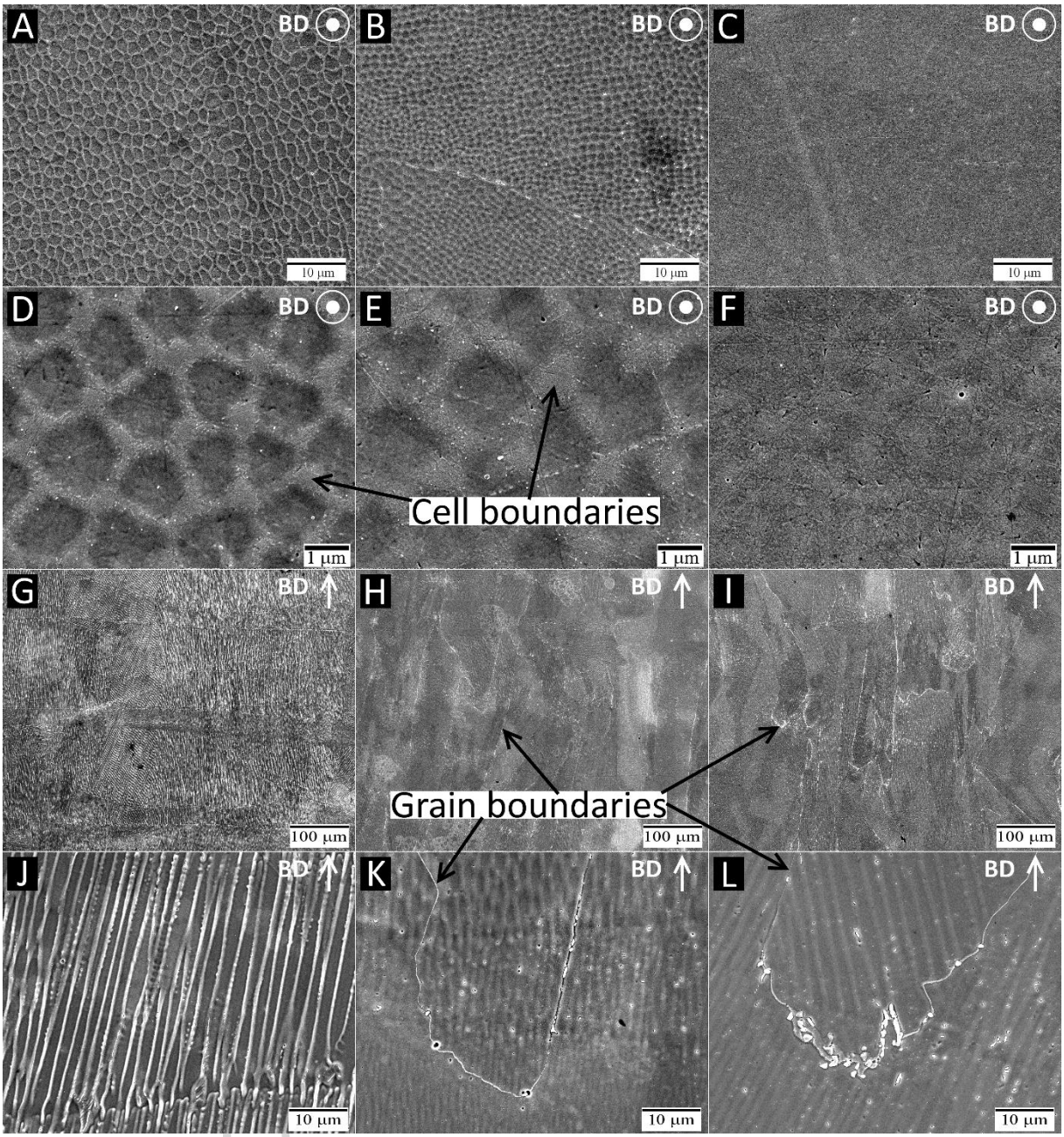

Figure 6. SEM images of the etched, as-manufactured sample; in a top-down view of: (A),(D) the top surface of the sample, (B),(E) the sample 5mm from the top, (C),(F) the sample 10mm from the top; in a side view of: (G),(J) the top part of the sample, (H),(K) the sample 10mm from the top, (I),(L) the sample 20mm from the top.

There are three different possible explanations for this phenomenon with the EBM® - manufactured stainless steel.

Firstly, the continuous background heating during the process keeps the entire part at a temperature of around 800°C, which is close to typical annealing temperatures used for 316L steel. This can have an extensive effect on the microstructure of the part. The further down from the top layers of the part, the longer time the material has been kept at this temperature and thus the influence on the material structure should be more significant.

Secondly, when a new layer is added and melted with the electron beam, several of the previously melted layers are also affected by the beam and re-melted one, or more time. If this

would be the primary reason for the differences in the microstructure, only the topmost few layers that have not been re-melted as many times as the rest of the sample will display a different structure. Figures 6G-L plainly illustrate the heterogeneity in the microstructure along the top 20 mm of the sample manufactured with the layer thickness of 0.07 mm. Thus, this is not the primary reason of the long-range heterogeneity in the sample materials microstructure.

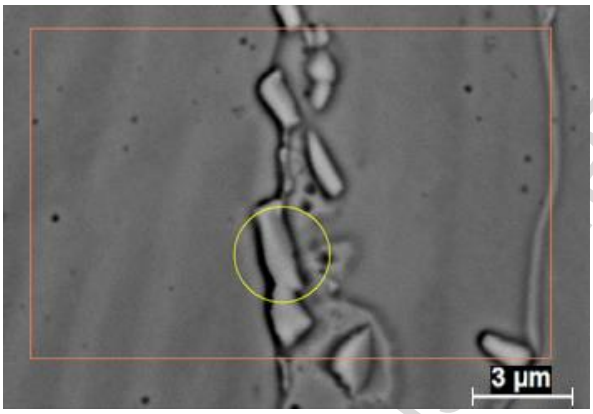

Figure 7. EDS results from the area inside the yellow circle.

Table 2. EDS Elements distribution results

Elements	Fe	Cr	Ni	Mo	Mn	Si
wt. %	63.0	21.5	8.8	5.0	1.1	0.6

Thirdly, with each new layer, the electron beam melts the new layer on top of the previously built part. When the melting happens, it significantly increases the temperature of the upper component layers and causes the heat wave to travel downwards. Thus temperature in the manufactured component is constantly oscillating around annealing temperature, periodically pushing the temperature to above 800 °C. Moreover, the exact temperature dynamics would be strongly dependent on the exact sample geometry and dimensions.

Table 3. Diffusion speed of Molybdenum in Austenite[16].

Temperature [°C]	Diffusion speed [nm/day]
820	1
950	30
1100	680

Table 3 shows typical Molybdenum diffusion rates in Austenite at different temperatures. At 820°C, the diffusion rate is extremely slow which implies that with only the building plate heating and a build time of 20 hours the long-range heterogenic microstructure would not form. A higher temperature is needed to initiate any significant diffusion of the Molybdenum. This implies that the oscillating raising- and falling of the temperature with each newly scanned layer has an essential role in this phenomenon.

3.5 Molybdenum precipitates

Performing EDS mapping on the cell boundaries at different sample heights consolidates the fact that the molybdenum is diffusing away from the cell boundaries. Figure 8 presents color-coded EDS images of the polished sample allowing for element ratio analysis. At the top surface of the sample (Figure 8A), the contrast difference between the cell boundaries and the middle of the cells is clear, indicating a difference in chemical composition between these areas. Looking at the color-coded image shows more significant amounts of Molybdenum along the cell boundaries compared to the inner part. The picture changes significantly for the layers 20 mm down from the upper sample surface (Figure 8B), the contrast is not as pronounced, and the cells are not as distinguishable. The EDS map also shows a good distribution of Molybdenum throughout the sample in this area. This reinforces the conclusion that molybdenum is diffusing through the sample during the manufacturing process. Also, from Figure 6 it is possible to note that the cell boundaries get thicker further down from the sample top, which implies that some of the molybdenum is diffusing towards the inner parts of the cells. The diffusion distances seem to be in the order of only a few nanometers, a very short distance, but it is still too far to be explained by the rates that should result in 1 nm/day. At the same time, a significant amount of molybdenum was detected as a precipitate in the grain boundaries. For substantial amounts to amass like this within the grain boundaries, it would need to diffuse over long distances through the cell, and grain boundaries in the sample. Indeed, it is known that diffusion through grain boundaries is significantly faster than diffusion through the bulk material [17], but no research has been done on diffusion through cell boundaries. From the results that the Molybdenum is accumulated in the cell boundaries, and later gathers in the grain boundaries, it is apparent that diffusion through the cell boundaries also has a lower energy threshold than for diffusion through the bulk. The Molybdenum has to move from the cell boundaries to the grain boundaries; the distance is up to several tenths of micrometers. The reason for the quicker diffusion through the grain boundaries is explained by the high number of dislocations in the area. The fact that Molybdenum also appears to have fast diffusion through the cell boundaries imply that there is also a high concentration of dislocations in that area, this has been shown before to be the case for SLM samples[9,18]. The way these dislocation networks form can be ascribed to the fast solidification of the material as discussed in section 3.2, as the material does not have time to attain a local chemical equilibrium, and therefore many dislocations will form in the areas with high Molybdenum concentration.

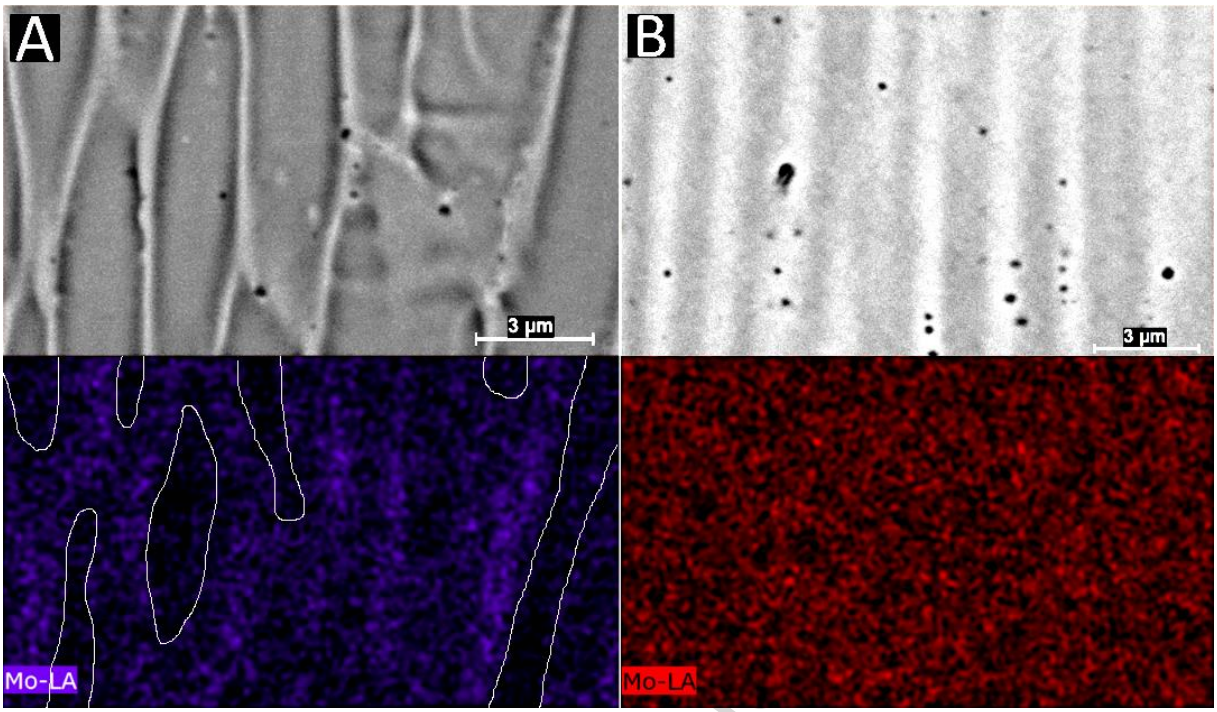

Figure 8. EDS analysis of the cell boundaries of; (A) the top surface where marked areas have a lesser amount of Mo, corresponding to the insides of the cells, (B) 20mm from the top.

3.6 Microhardness

Microindentation analysis was performed for three different areas of the samples (Table 4) with 12 indentations in each area. There is no noticeable difference in the microhardness between the different areas in the sample. The hardness values measured are lower than what is achieved in specimens prepared by SLM process and are closer to what is measured for the commonly HIPed material (around 170HV). The reason for this difference in hardness between EBM and SLM manufactured samples is the greater segregation of molybdenum in SLM as well as the formation of a lot of small precipitates during SLM[19,20].

Table 4. Hardness at different areas

Area	Hardness 1kgf [HV]
Top	161±11
10mm from the top	157±10
40mm from the top	164±13

4. Conclusions

The continued heating and re-melting of the material during the EBM process generates a complex annealing effect, depending both on the process parameter settings, and on the particular component geometry and orientation in the build, that homogenizes the microstructure. The cellular structure initially formed by rapid solidification appears less and less pronounced further from the top of the sample, and simultaneously the grain boundaries become more and more pronounced. At the parts of the component further from the top, molybdenum has diffused away from the cell boundaries into the cells and the grain boundaries by forming molybdenum-rich precipitates. The implication of this observation is

that diffusion through cell boundaries might be similar to diffusion through grain boundaries, which is known to be faster than diffusion through the bulk material. Despite the local enrichment of molybdenum in cell boundaries and grain boundaries, austenite is observed as the dominating phase throughout the entire sample, with less than 0.5% other phases. No differences in microhardness were detected at different sample locations.

Acknowledgments

This work was supported by the Fusion for Energy, the European Union's joint undertaking for ITER and the Development of Fusion Energy, and Vinnova, Swedish Governmental Agency for Innovation Systems. This publication reflects the views of the authors only, and Fusion for Energy or Vinnova may not be held accountable for any use which may be made of the information therein. Authors would like to thank Dianzheng Wang at School of Materials Science & Engineering at Tsinghua University, China, who performed all EBSD measurements.

Data availability

All the data required to reproduce these experiments are present in the article.

References

[1] I. Campbell, D. Bourell, I. Gibson, Additive Manufacturing: Rapid Prototyping comes of age, Rapid Prototyp. J. 18 (2012) 255–258. doi:10.1108/13552541211231563.

[2] A.A. Shapiro, J.P. Borgonia, Q.N. Chen, R.P. Dillon, B. McEnerney, R. Polit-Casillas, L. Soloway, Additive Manufacturing for Aerospace Flight Applications, J. Spacecr. Rockets. 53 (2016) 952–959. doi:10.2514/1.A33544.

[3] Y.S. Hedberg, B. Qian, Z. Shen, S. Virtanen, I. Odnevall Wallinder, In vitro biocompatibility of CoCrMo dental alloys fabricated by selective laser melting, Dent. Mater. 30 (2014) 525–534. doi:10.1016/j.dental.2014.02.008.

[4] Y. Zhong, L.-E. Rännar, L. Liu, A. Koptyug, S. Wikman, J. Olsen, D. Cui, Z. Shen, Additive manufacturing of 316L stainless steel by electron beam melting for nuclear fusion applications, J. Nucl. Mater. 486 (2017) 234–245. doi:10.1016/j.jnucmat.2016.12.042.

[5] Y. Zhong, L.-E. Rännar, S. Wikman, A. Koptyug, L. Liu, D. Cui, Z. Shen, Additive manufacturing of ITER first wall panel parts by two approaches: Selective laser melting and electron beam melting, Fusion Eng. Des. 116 (2017) 24–33. doi:10.1016/j.fusengdes.2017.01.032.

[6] N.B. Qi, Y.N. Yan, F. Lin, W. He, R.J. Zhang, Direct metal part forming of 316L stainless steel powder by electron beam selective melting, Proc. Inst. Mech. Eng. Part B (Journal Eng. Manuf. 220 (2006) 1845–1853. doi:10.1243/09544054jem438.

[7] Y. Zhong, L. Liu, S. Wikman, D. Cui, Z. Shen, Intragranular cellular segregation network structure strengthening 316L stainless steel prepared by selective laser

melting, J. Nucl. Mater. 470 (2016) 170–178. doi:10.1016/j.jnucmat.2015.12.034.

[8] K. Saeidi, X. Gao, Y. Zhong, Z.J.J. Shen, Hardened austenite steel with columnar sub-grain structure formed by laser melting, Mater. Sci. Eng. A. 625 (2015) 221–229. doi:10.1016/j.msea.2014.12.018.

[9] Y.M. Wang, T. Voisin, J.T. McKeown, J. Ye, N.P. Calta, Z. Li, Z. Zeng, Y. Zhang, W. Chen, T.T. Roehling, R.T. Ott, M.K. Santala, P.J. Depond, M.J. Matthews, A. V Hamza, T. Zhu, Additively manufactured hierarchical stainless steels with high strength and ductility, Nat. Mater. (2017). doi:10.1038/nmat5021.

[10] A. Keshavarzkermani, M. Sadowski, L. Ladani, Direct metal laser melting of Inconel 718: Process impact on grain formation and orientation, J. Alloys Compd. 736 (2018) 297–305. doi:10.1016/j.jallcom.2017.11.130.

[11] M.R.R. Dadfar, M.H.H. Fathi, F. Karimzadeh, M.R.R. Dadfar, A. Saatchi, Effect of TIG welding on corrosion behavior of 316L stainless steel, Mater. Lett. 61 (2007) 2343–2346. doi:10.1016/j.matlet.2006.09.008.

[12] A.A. Antonysamy, J. Meyer, P.B. Prangnell, Effect of build geometry on the β-grain structure and texture in additive manufacture of Ti6Al4V by selective electron beam melting, Mater. Charact. 84 (2013) 153–168. doi:10.1016/j.matchar.2013.07.012.

[13] A. Basak, S. Das, MR46CH06-Das Epitaxy and Microstructure Evolution in Metal Additive Manufacturing, Annu. Rev. Mater. Res. 46 (2016) 125–49. doi:10.1146/annurev-matsci-070115-031728.

[14] X. Zhou, K. Li, D. Zhang, X. Liu, J. Ma, W. Liu, Z. Shen, Textures formed in a CoCrMo alloy by selective laser melting, J. Alloys Compd. 631 (2015) 153–164. doi:10.1016/j.jallcom.2015.01.096.

[15] I. Yadroitsev, P. Krakhmalev, I. Yadroitsava, S. Johansson, I. Smurov, Energy input effect on morphology and microstructure of selective laser melting single track from metallic powder, J. Mater. Process. Technol. 213 (2013) 606–613. doi:10.1016/j.jmatprotec.2012.11.014.

[16] J.D. VERHOEVEN, STEEL METALLURGY FOR THE NON-METALLURGIST, ASM International, Ohio, 2007.

[17] A. Atkinson, Grain-boundary diffusion: an historical perspective, J. Chem. Soc. Faraday Trans. 86 (1990) 1307–1310. doi:10.1039/FT9908601307.

[18] K. Saeidi, X. Gao, F. Lofaj, L. Kvetková, Z.J. Shen, Transformation of austenite to duplex austenite-ferrite assembly in annealed stainless steel 316L consolidated by laser melting, J. Alloys Compd. 633 (2015) 463–469. doi:10.1016/j.jallcom.2015.01.249.

[19] L. Liu, Q. Ding, Y. Zhong, J. Zou, J. Wu, Y.L. Chiu, J. Li, Z. Zhang, Q. Yu, Z. Shen, Dislocation network in additive manufactured steel breaks strength-ductility trade-off, Mater. Today. (2017). doi:10.1016/j.mattod.2017.11.004.

[20] S.-H.H. Kim, H. Kim, N.J. Kim, Brittle intermetallic compoundmakes ultrastrong low-density steelwith large ductility, Nature. 518 (2015). doi:10.1038/nature14144.

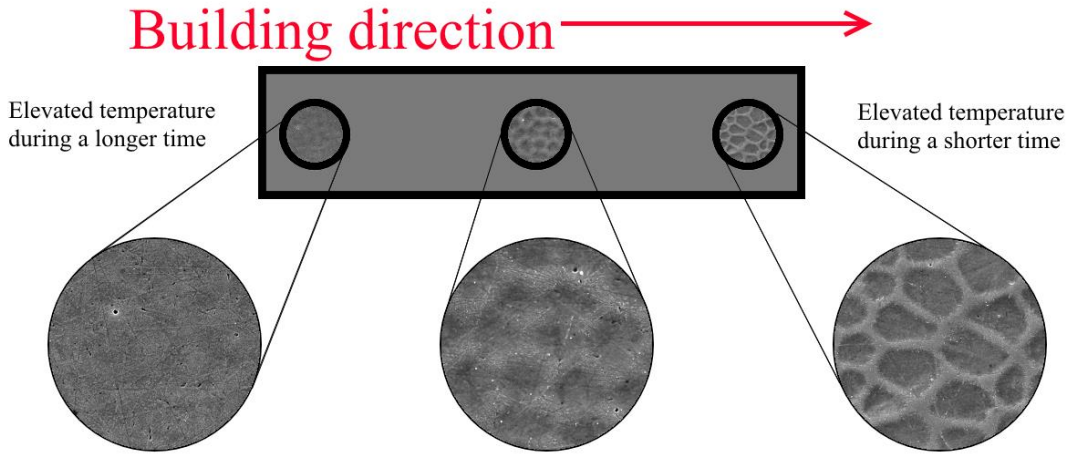

Graphical abstract

Highlights

- Electron beam melting manufactured parts has a complicated thermal history.
- The microstructure varies with the position in the sample.
- Pronounced Molybdenum segregation at the top disappears at the bottom.
- Fast molybdenum diffusion in cell boundaries as well as grain boundaries.